Implosion of a spherical shock wave reflected from a spherical wall

doi: 10.1017/S0022112005003587

J. Fluid Mech. (2005), *vol.* 530, *pp.* 223–239.
doi:10.1017/S0022112005003587 Printed in the United Kingdom

Implosion of a spherical shock wave reflected from a spherical wall

By S. H. R. HOSSEINI AND K. TAKAYAMA

Tohoku University Biomedical Engineering Research Organization, 2-1-1, Katahira, Aoba, Sendai 980-8577, Japan
hosseini@cerers.ifs.tohoku.ac.jp

(Received 8 March 2004 and in revised form 7 December 2004)

The paper describes results of experiments of a converging spherical shock wave reflected from a spherical wall. In order to visualize the motion and the flow field behind the shock waves, an aspheric lens-shaped transparent test section made of acrylic PMMA (polymethyl methacrylate) with an inner spherical cavity was designed and constructed. This test section made optical flow visualization with collimated object beams possible. Spherical shock waves were produced at the centre of the spherical cavity by explosion of silver azide pellets ranging from 1.0 to 10.0 mg with corresponding energies of 1.9 to 19 J. The charges were ignited by irradiation of a pulsed Nd:YAG laser beam. Pressures were also measured at two points with pressure transducers mounted flush at the inner wall of the test section. The pellet was simultaneously ignited on two sides or was shaped to produce a uniform diverging spherical shock wave. This spherically diverging shock wave was reflected from the spherical inner wall of the test section to form a converging spherical shock wave. We visualized the shock-wave motion by using double exposure holographic interferometry and time-resolved high-speed video recording. The sequence of diverging and converging spherical shock-wave propagations and their interaction with gaseous explosion products were observed. The convergence, acceleration and stability of the imploding shock wave in the test section were studied.

1. Introduction

The high pressures and temperatures attainable at the centre of imploding shock waves in gases, suggest various interesting scientific applications (Glass & Sislian 1994). Stability of converging cylindrical shock waves has been intensively studied experimentally and analytically. Nevertheless, production of uniform converging spherical shock waves in gases and their stability are still one of the unresolved problems in shock wave research.

Guderley (1942) analysed, for the first time, shock wave convergence and obtained a self-similar solution of converging cylindrical and spherical shock waves. Since then, Butler (1954) and Van Dyke & Guttmann (1982) have carried out analytical investigations regarding the self-similar character of converging shock waves. Stanyukovich (1960) reviewed the analytical investigations of shock-wave convergence. Gardner, Book & Bernstein (1982), Wang (1982), Schwendeman & Whitham (1987) and Schwendeman (2002) discussed the stability of converging shock waves. Payne (1957), Saito & Glass (1984) and Schwendeman (2002) performed numerical simulations of imploding shock waves.

Converging cylindrical shock waves were generated for the first time by Perry & Kantrowitz (1951) using an annular coaxial horizontal shock tube which consisted

of a teardrop-shaped inner core. They visualized converging shock waves by the schlieren method. Takayama, Kleine and Grönig (1987) observed, by using double-exposure holographic interferometry, the existence of mode three/four instability over converging cylindrical shock waves in the vicinity of the converging centre, which was generated in annular coaxial horizontal shock tubes having three/four struts supporting the inner core. To produce a uniform converging cylindrical shock wave, Watanabe, Onodera & Takayama (1995) constructed a vertical coaxial diaphragmless shock tube. This facility was later modified by Hosseini, Onodera & Takayama (1999) and was restricted to moderate shock-wave strength. Hosseini *et al.* (2000) constructed a compact vertical diaphragmless shock tube for creating uniformly converging shock waves. Apazidis & Lesser (1996) and Apazidis *et al.* (2002) studied the convergence of a polygonal shock wave, reflected from a two-dimensional cavity. Knystautas, Lee & Lee (1969) studied the imploding cylindrical detonation waves and reported that it was stable. Terao (1983) reported a similar result and generated high pressures by the focusing of detonation waves. However, it is not clear whether or not converging shock waves are stable.

Glass (1972) constructed a hemispherical implosion chamber and Saito & Glass (1982) succeeded in imploding a hemispherical shock wave at its centre. Extremely high pressures and temperatures were generated at the focal zone in proportion to the amount of energy released, but the stability of imploding shock waves was not discussed.

In the present study, micro-explosives were detonated at the centre of a spherical chamber and the resulting reflected spherical shock wave converged toward the centre, free of any disturbances due to shock wave propagation over a solid wall. The present complete spherical chamber with an aspheric outer wall was made of transparent acrylic PMMA (polymethyl methacrylate) to enable the use of optical flow visualization as an inherently non-disruptive diagnostic method.

2. Experimental method

2.1. *Test section*

To observe the effects of secondary gas injection into a conical supersonic nozzle flow and to study gas injection thrust vector control, Yamanaka (1972) designed a nozzle made of glass having a circular inner cross-section and an aspheric outer wall contour. We have adopted Yamanaka's method and we have observed shock waves and flows in circular cross-section shock tubes by using aspheric cylindrical straight test sections (Takayama 1983; Hosseini & Takayama 2001).

We constructed, as an extension of previous cylindrical test sections, a transparent spherical test section of 150 mm inner diameter with an aspherical outer wall of dimensions 270 mm and 203.3 mm. The test section was made of acrylic PMMA. Figure 1(*a*) shows the aspheric test section and its schematic light-ray tracings. This shape permits the collimated visualization light to traverse the test section as a parallel contracted beam, and to emerge as a parallel re-expanded beam. The shape of the test section was obtained by applying Snell's refraction law to the light rays,

$$\frac{S}{S_0} = \frac{n\cos\theta + \cos\psi}{(n+1)\cos\psi}, \quad \sin\psi = n\sin\theta, \tag{1}$$

where s, s_0, n and θ are wall thickness, maximum wall thickness, refractive index and the light-ray angle defined in figure 1(*a*), respectively. The value of the refractive index for acrylic PMMA was determined experimentally by Takayama (1983) using five

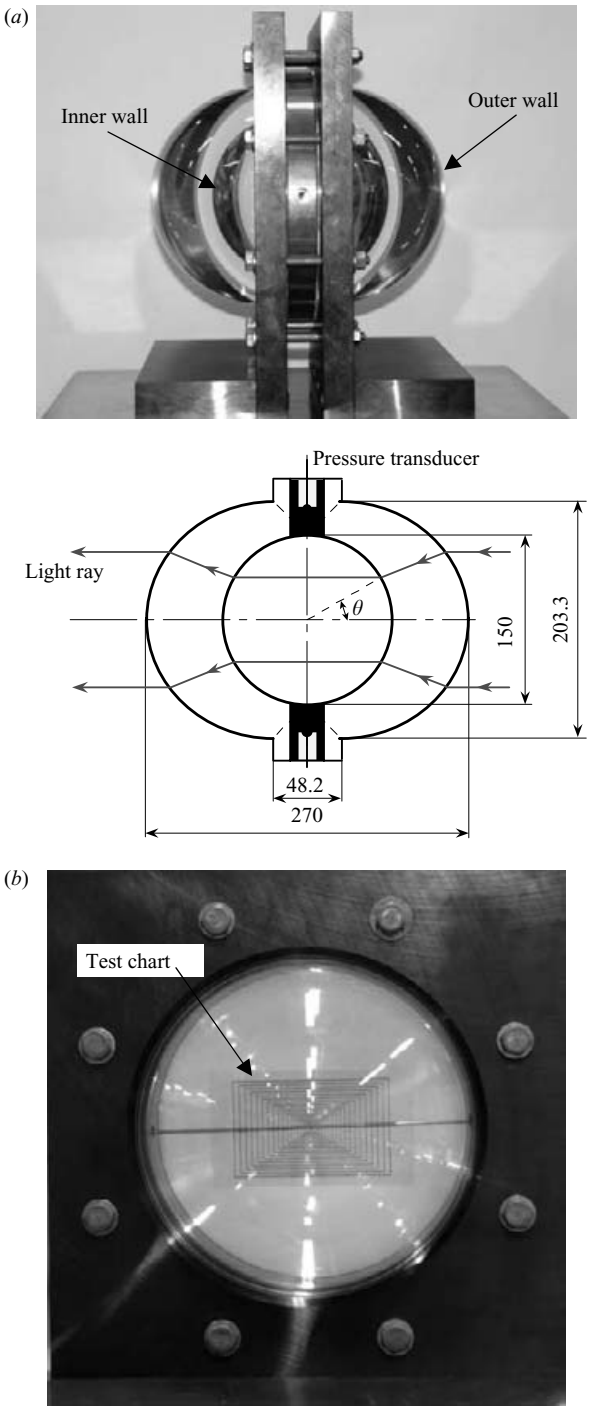

FIGURE 1. (*a*) Photograph of 150 mm inner diameter aspherical transparent test section with a schematic diagram of the visualization light rays in the test section. (*b*) The front view shows transparency of the test section.

different wavelength argon-ion and He–Ne lasers. For each wavelength, the refractive index was measured and for the wavelength of the ruby laser 694 nm it was calculated to be 1.491.

After machining, the test section was thoroughly polished by hand. Although locally the wall thickness deviates very slightly from the designed value, it does not degrade the results when double-exposure holographic interferometry or shadowgraph visualization is applied. Figure 1(*b*) shows an observed image of a test chart inserted in the centre of the test section. The image is enlarged by a factor of 1.36 and its distortion is negligibly small.

To generate spherical shock waves, silver azide pellets (AgN_3, 99.9% purity; 3.77 g cm^{-3}, Chugoku Kayaku Co. Japan) ranging from 1.0 to 10.0 mg ($\pm$1% scatter in mass) were detonated at the centre of the test section. The 10 mg charges had a cylindrical shape of 1.5 mm diameter, and were 1.5 mm long (Nagayasu 2001). The pellet was glued to the polished end of a 0.6 mm core diameter optical fibre and was ignited by irradiation of a Q-switched Nd:YAG laser beam of 1064 nm wavelength, 7 ns pulse duration, 3.2 mm diameter beam, total energy 25 mJ per pulse. The total energy of 10 mg pellet is about 19 J, whereas less than 1 mJ of laser energy is used for the ignition. The minimum energy required to ignite the silver azide pellet is 0.10 mJ (Mizukaki 2001). The shape of the shock wave, immediately after the explosion of the pellet, is never spherical, but shows a three-dimensionally deformed shape (Kleine *et al.* 2003). With propagation, it rapidly converts to a spherical shape which implies that the diverging shock wave is always stable. However, at the moment of ignition, many minute fragments are ejected from the pellet's surface. These fragments overtake the shock wave at supersonic speed, much faster than the shock speed in air. Conical 5.0 mg pellets were produced out of 10 mg charges by shaping them with a sharp bamboo blade. The shape of 1.0 and 2.0 mg silver azide charges was irregular.

Pressures were measured with piezo-electric pressure transducers (Kistler model 603B1), which were mounted flush at the inner wall of the test section, as shown in figure 1(*a*). This arrangement was intended to identify, within the response time of the transducers, whether or not the spherical shock wave arrived at these pressure transducers simultaneously. Since the pressure transducer has a nominal radius of 2.77 mm which is small compared to the 75 mm radius of the test section, the reflection of the incident shock from the pressure transducers and the test section wall was nearly uniform.

2.2. *Flow visualization*

Double-exposure holographic interferometry was used for quantitative flow visualization (Takayama 1983). Figure 2(*a*) shows a schematic diagram of the optical set-up. The optical arrangement consists of two parabolic schlieren mirrors of 1000 mm dia. and 8.0 m focal length. A beam splitter (BS) transmitted 50 % of the source light intensity to an object beam (OB) and 50 % to a reference beam (RB). Plane mirrors (M) were used to produce two light paths OB and RB of identical length. The light source was a double pulse ruby laser (InnoLas HLS/R20, 694 nm wavelength, 20 ns pulse duration, 1 J per pulse). The source laser beam was diverged with a lens (L), collimated with the parabolic mirror, and pointed to illuminate the test section. As seen in figure 2(*a*), the image of the phenomenon in the test section was focused with a focusing lens and was collected on a holographic film placed on a film holder (FH). The object and reference beams were then superimposed on the holographic film. Double exposure of the ruby laser was used. The first laser exposure was carried out before triggering the micro charges and the second exposure was synchronized with

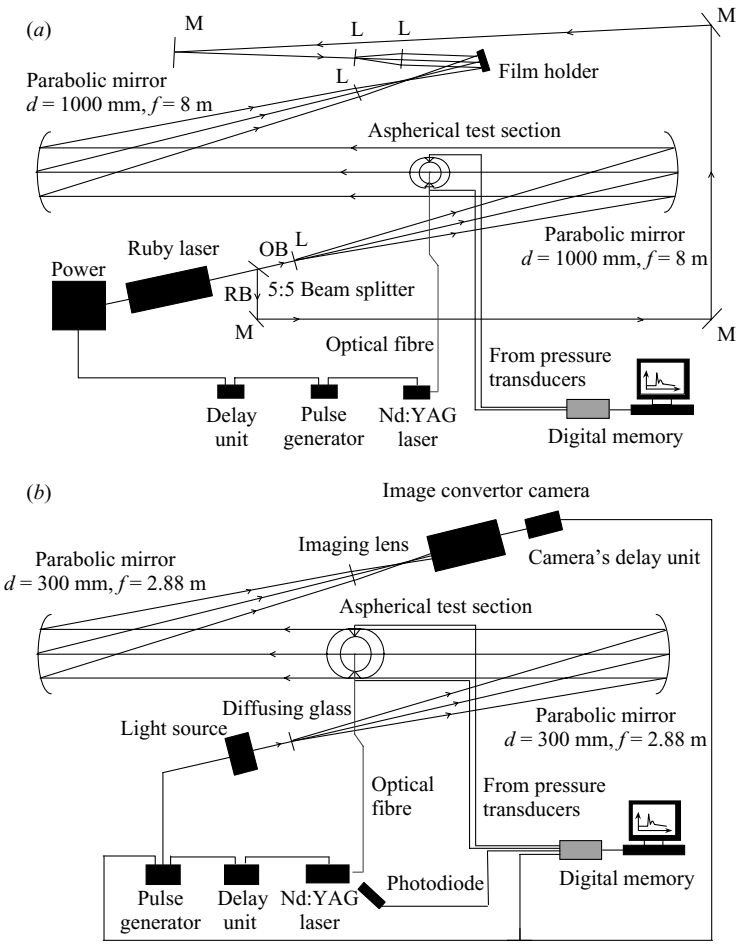

FIGURE 2. (*a*) Double exposure holographic interferometric optical set-up. L, lens; M, mirror; OB, object beam; RB, reference beam. (*b*) Schematic diagram of optical set-up for time-resolved high-speed shadowgraph visualization.

the propagation of the shock wave in the test section with an appropriate delay time. The holograms thus constructed were later reconstructed by illuminating them with an argon-ion laser beam (514.5 nm wavelength and 1 watt) through an optical set-up, which was nearly the same as the optical set-up of the reference beam.

The insertion of any transducer inside the test section would interfere with the shock front and disturb the flow behind it. Therefore, an optical non-disruptive diagnostic of the converging spherical shock wave is the preferred method. We performed, in addition to high spatial resolution, single-shot holographic interferometry, high-speed time-resolved visualizations based on the shadowgraph method.

Figure 2(*b*) shows a schematic diagram of the optical set-up for the shadowgraph flow visualization. A flash-lamp was used as an intense light source. The source light was diffused and diverged by transmitting through a diffusing glass plate, collimated by a 300 mm diameter parabolic mirror, and illuminated the test section. By using image converter cameras (Imacon 468 and Ultra 8, DRS Hadland) eight images were recorded in each experiment. In order to visualize the entire sequence of shock-wave convergence, a high-speed video camera (ISIS prototype, Shimadzu Co.) was

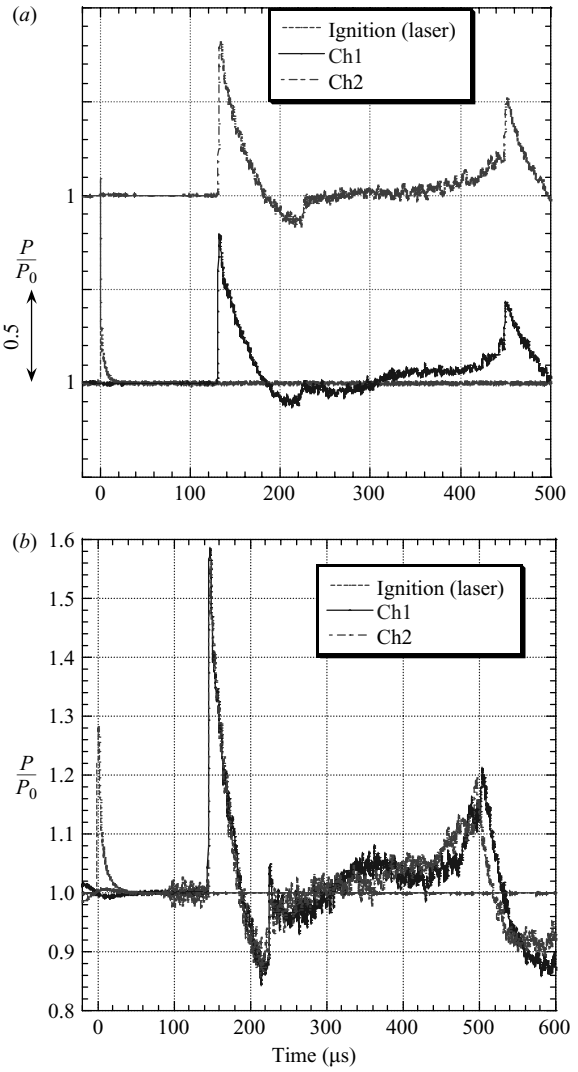

FIGURE 3. Pressure histories measured at the test section and normalized by the initial pressure: (*a*) after explosion of a 10.0 mg cylindrical silver azide pellet, $P_0 = 100.65$ kPa; (*b*) after explosion of a 5.0 mg conical silver azide pellet, $P_0 = 101.35$ kPa.

employed. This camera could record 100 sequential images in a single experiment at 1 000 000 frames per second (Etoh 2002). Simultaneously with the holographic interferometric and time-resolved shadowgraph visualizations, wall pressures (Ch1, Ch2) were measured and recorded.

3. Results and discussion

3.1. *Pressure measurement*

Figure 3(*a*) shows pressure histories, normalized by the initial pressure, following the detonation of a 10 mg silver azide pellet in air at initial pressure $P_0 = 100.65$ kPa. As seen in the experimental set-up of figure 1(*a*), pressure transducers Ch1 and Ch2 can record reflected pressures. A photodiode was used to monitor the irradiation of the

Nd:YAG laser beam which ignited the pellets. The ignition delay of silver azide was found to be less than 1 μs (Mizukaki 2001). The monitored signal indicates the time instant of explosion and was used as a time base to measure the arrival time of the diverging shock wave at the inner wall of the test section. In figure 3(*a*), 128 μs after the ignition, the diverging shock wave arrived at the inner wall producing a steep pressure jump. From the Rankine–Hugoniot relations, assuming a planar shock wave reflected from a wall (Baker 1973), the side-on pressure can be evaluated from:

$$\Delta P_r = 2\Delta P_s + \left\{\left[(\gamma+1)\Delta P_s^2\right]/[(\gamma-1)\Delta P_s + 2\gamma]\right\}, \tag{2}$$

where $\Delta P_r = (P_r - P_0)/P_0$, $\Delta P_s = (P_s - P_0)/P_0$, P_r and P_s are reflected and side-on pressures. In figure 3(*a*), the normalized reflected shock pressure has a value of 1.8, which gives the shock or side-on pressure of 1.35. This corresponds to incident diverging shock-wave Mach number $M_s = 1.14$ at the test section wall. Pressure signals of the two pressure transducers are nearly identical with respect to both magnitude and arrival time of the diverging shock wave. This confirms, within the response time accuracy of the transducers, that the explosion took place at the centre of the test section. A small pressure jump at 222 μs apparently corresponds to a secondary shock wave, produced by the merging of compression waves due to overexpansion following the propagating of rarefaction waves into the explosion products gas. The primary shock wave reflected from the test section and converged. After its reflection from the centre, it arrived at the test section inner wall at 448 μs. A similar trend of pressure time-history was observed for reduced charge mass of 5.0, 2.0 and 1.0 mg. Figure 3(*b*) shows pressure histories for detonation of a 5.0 mg conical pellet measured simultaneously with flow visualization of figure 9. The diverging shock wave arrived at the inner wall at 145 μs after the ignition. A normalized reflected pressure of 1.57 was measured, corresponding to an incident shock Mach number of 1.105 at the test section wall.

3.2. *Flow visualization*

Figure 4 shows infinite fringe interferograms of the explosion of 10.0 mg cylindrical silver azide pellets in air at 100.2 kPa. The temporal accuracy of sequential interferograms is 1 μs. Figure 4(*a*) shows the spherical shock wave, 50 μs after the explosion. A solid line visible from the top to the centre is the optical fibre. A number of fragments flying ahead of the shock wave at supersonic speed are clearly visible in the upper part of figure 4(*a*). The detonation wave propagating in the cylindrical silver azide in the direction of the laser irradiation takes a time interval of several hundred picoseconds, which affects not only the spherical shape of the diverging shock wave, but also the number and the direction of the ejected fragments. The particles consisted of debris of glue and unburned silver azide, which were driven and accelerated outward by the expanding detonation gases. These fragments are accompanied by conical shock waves, as can be observed in figure 4(*a*). The inclination angles of the conical shocks of the fragments corresponded to their free flight speed. In figure 4(*b*) at 100 μs, the diverging shock wave and the secondary shock wave are clearly observed. Fringes generally correspond to isopycnics or isodensity contours in two-dimensional flows. However, in axial or in point symmetric flows, they show density variation across the test section integrated in the direction of the object beam. The fringes between the diverging shock wave and the secondary shock look nearly concentric, which implies that density decreased from the diverging shock to the secondary shock, consistent with the pressure histories as seen in figure 3(*a*). The gaseous detonation products of the cylindrical charge have a disk shape in the circumferential direction with a

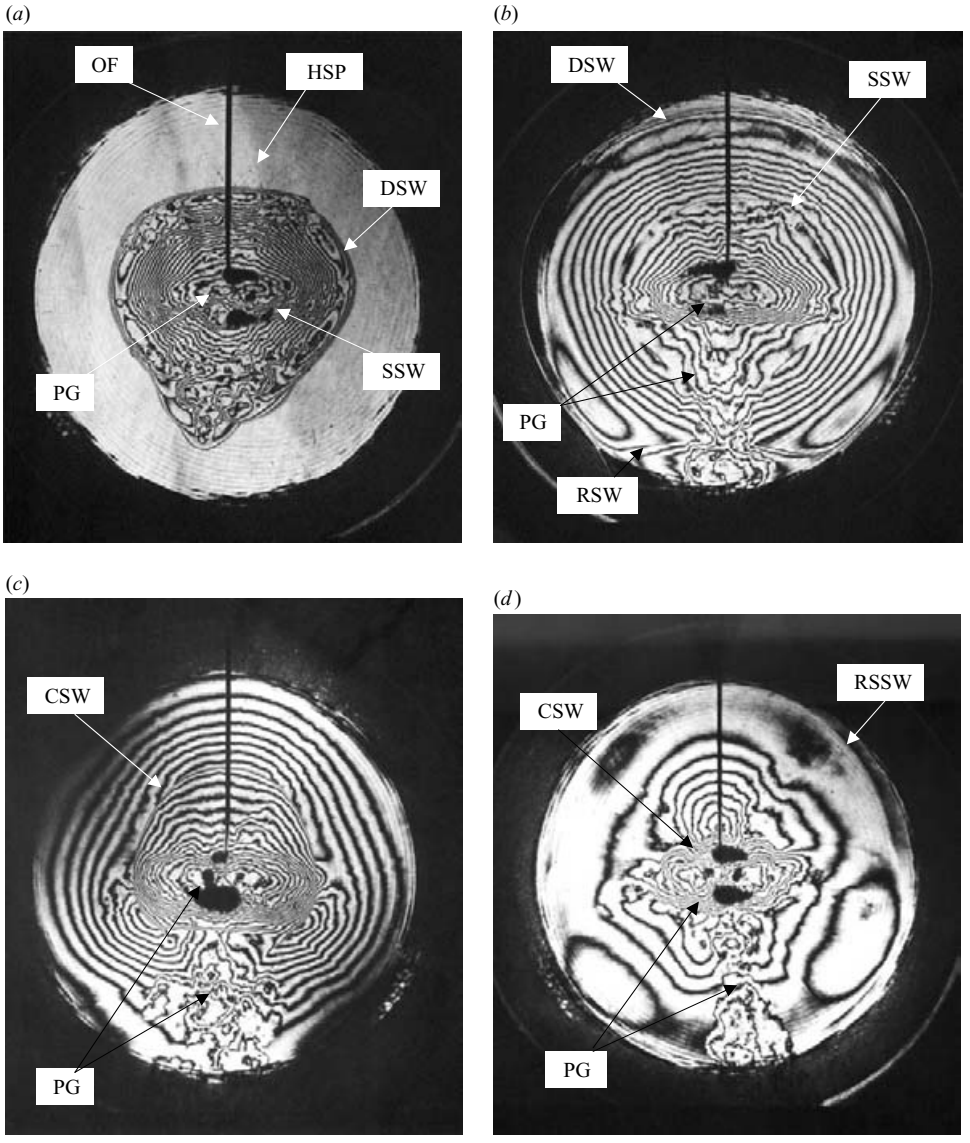

FIGURE 4. Sequential infinite fringe interferograms of diverging and converging shock waves produced by explosion of 10.0 mg cylindrical silver azide charges at ambient pressure 100.2 kPa. CSW, converging shock wave; DSW, diverging shock wave; HSP, high-speed particles; OF, optical fibre; PG, product gases; RSW, reflected shock wave; RSSW, reflected secondary shock wave; SSW, secondary shock wave. (*a*) 50 μs; (*b*) 100 μs; (*c*) 260 μs; (*d*) 290 μs.

jet shape leading front in the axial igniting direction (Kleine *et al.* 2003). In the lower part of figure 4(*b*), the jet of gaseous detonation products affected the spherical flow field, and the leading or disturbed part of the shock wave in that direction has reflected from the test section and would decisively affect symmetrical implosion of the primary reflected shock wave seen in figure 4(*c–d*).

To produce uniform spherically diverging shock waves without forming the jet of gaseous detonation products, a simultaneous two-sided ignition of a 10 mg pellet was employed. By splitting the Nd:YAG laser beam into two and transmitting through

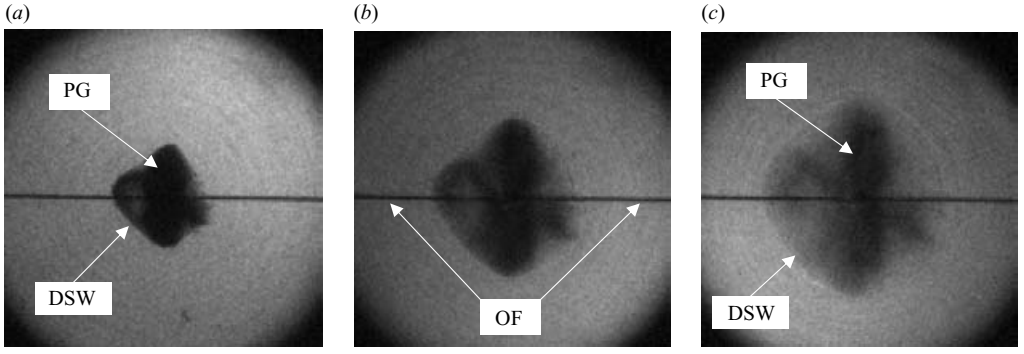

FIGURE 5. Three frames of time-resolved shadowgraph visualization of diverging spherical shock wave induced by two-base ignition of 10.0 mg cylindrical silver azide pellet in air at ambient pressure 100.65 kPa. DSW, diverging shock wave; OF, optical fibres; PG, product gases. (*a*) 12 μs; (*b*) 28 μs; (*c*) 44 μs.

two optical fibres, the 10.0 mg cylindrical charges were ignited simultaneously on their two bases. Figure 5 shows three images selected from eight sequential high-speed shadowgraph visualizations of a two-sided ignited pellet. Each frame had a 200 ns exposure time with 8 μs inter-frame time. A more uniform spherically diverging shock wave was obtained. Figure 6 shows nine images picked out of 100 frames of the time-resolved high-speed video images of the converging spherical shock wave with 2 μs inter-frame time and 250 ns exposure time. In figures 5 and 6, the gaseous products generated by the detonation of cylindrical pellets formed a disk-shaped cloud. When the imploding shock wave propagated through the high-temperature cloud, it assumed an elliptical shape rather than keeping its spherical shape. This resulted in two separate focusing points 20 mm apart, as seen in figure 6(*i*). To overcome this defect, 2.0 and 1.0 mg irregular shaped charges were detonated by a method similar to the single-base ignition. Experiments were also performed with 5.0 mg base-ignited conical pellets.

Results of the evaluation of time-resolved images are shown in figure 7. Figure 7(*a*) shows the variation of the averaged diverging shock Mach number with the normalized radius ($R_0 = 75$ mm radius of the test section). The shock Mach number at the test section wall ($R/R_0 = 1$) was estimated from the value of pressure measurements. Figure 7(*b*) shows the deviation of the shock front from a spherical shape ($\Delta R = |R - R_{av}|$), normalized by the test section radius. As the diverging shock wave propagates and its radius increases, the shock Mach number decreases and the shock approaches a spherical shape, which is consistent with explosion-driven diverging shock waves being stable.

Figure 8 shows a diverging shock wave produced by base ignition of a 5.0 mg conical pellet with 2 μs inter-frame time and 250 ns exposure time. A uniform diverging spherical shock wave was produced as observed sequentially in figure 8(*g–i*). In figure 8(*c*), as in figure 4(*a*), a number of minute fragments accompanied by conical shock waves are observed. When the fragments impacted on the inner wall, they caused some pitting damage on the transparent test section. Temperatures behind the conical shock wave generated by these fragments were so elevated that a belated ignition of these explosive fragments was caused. Among high-speed video images this phenomenon was observed in figure 8(*g*). Figure 9 shows a time-resolved shadowgraph of the convergence of a spherical shock wave reflected from the test section wall. A hundred sequential images were recorded with 2 μs inter-frame time and 250 ns exposure time.

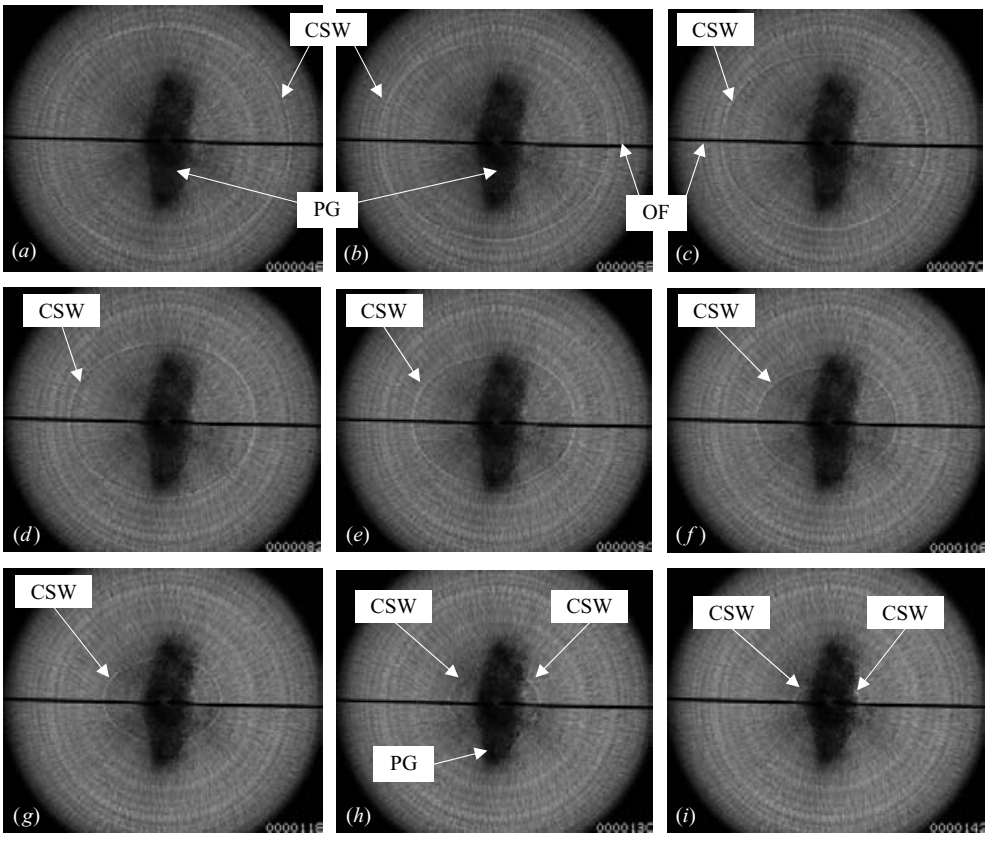

FIGURE 6. Nine frames of time-resolved high-speed shadowgraph visualization of converging spherical shock wave after reflection from the test section, produced by two-base ignition of 10.0 mg cylindrical silver azide charge in air at ambient pressure 100.65 kPa: (*a*) 192 μs; (*b*) 204 μs; (*c*) 216 μs; (*d*) 228 μs; (*e*) 240 μs; (*f*) 252 μs; (*g*) 264 μs; (*h*) 276 μs; (*g*) 288 μs. CSW, converging shock wave; OF, optical fibres; PG, product gases.

The converging shock kept its spherical shape up to 285 μs, however, after this time, it interacted with gaseous explosion products and started to become slightly disturbed.

The converging shock wave interacted with the interface between the gaseous detonation products and the shocked air and an intensified mixing was observed at a later time. It would be worth conducting Richtmyer–Meshkov (RM) instability studies in which a spherical shock wave interacts with a concentric discontinuous gaseous interface filled with heavy or light gas in this aspheric test section. If visualization of such an impulsively accelerated interface is carried out, the interface deformation would represent RM instability free from the interference of any solid boundary. For this purpose, a 300 mm inner diameter aspheric transparent test section is being constructed.

A wave diagram for the diverging and the converging spherical shock waves was drawn from evaluation of the time-resolved video recording for 5.0 mg conical pellets and is shown in figure 10. The propagation of the secondary shock wave in the test section is also shown in this figure. The diverging shock wave decelerates and reflects from the spherical wall at 145 μs. The secondary shock wave is very weak and propagates at a constant velocity of 350 m s^{-1}, close to the sound speed of air 346.3 m s^{-1} at

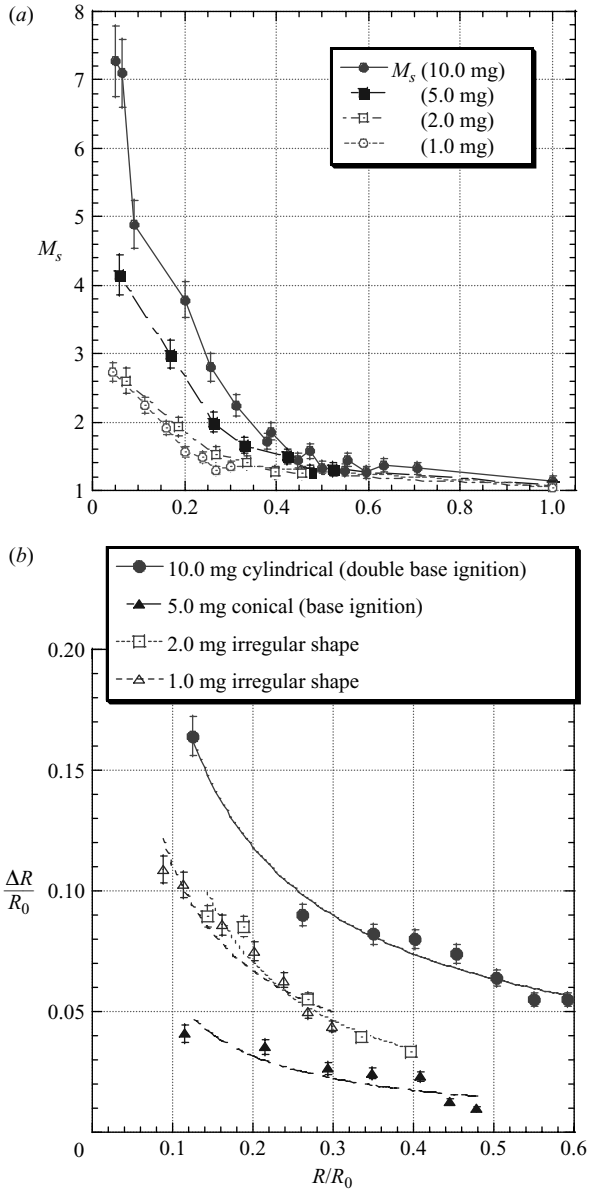

FIGURE 7. (*a*) Variation of diverging shock wave Mach number with radius, (*b*) deviation of diverging shock front from spherical shape; deduced from time-resolved visualizations.

the experimental room temperature of 298 K. The converging shock wave accelerates toward the centre of convergence and increases in strength with propagation. Experimental results are compared with a numerical prediction by solving one-dimensional Eulerian equations combined with the revised Kihara–Hikita equation of state for the detonation of silver azide (Tanaka 1986, 2000). A good agreement of the shock wave trajectory between the experiment and the numerical prediction was obtained. A detailed description of the numerical method was reported by Tanaka (1986, 2000).

Figure 11 shows the deviation ΔR of the shock front from a spherical shape normalized by the mean radius R of the converging shock wave. The deformation

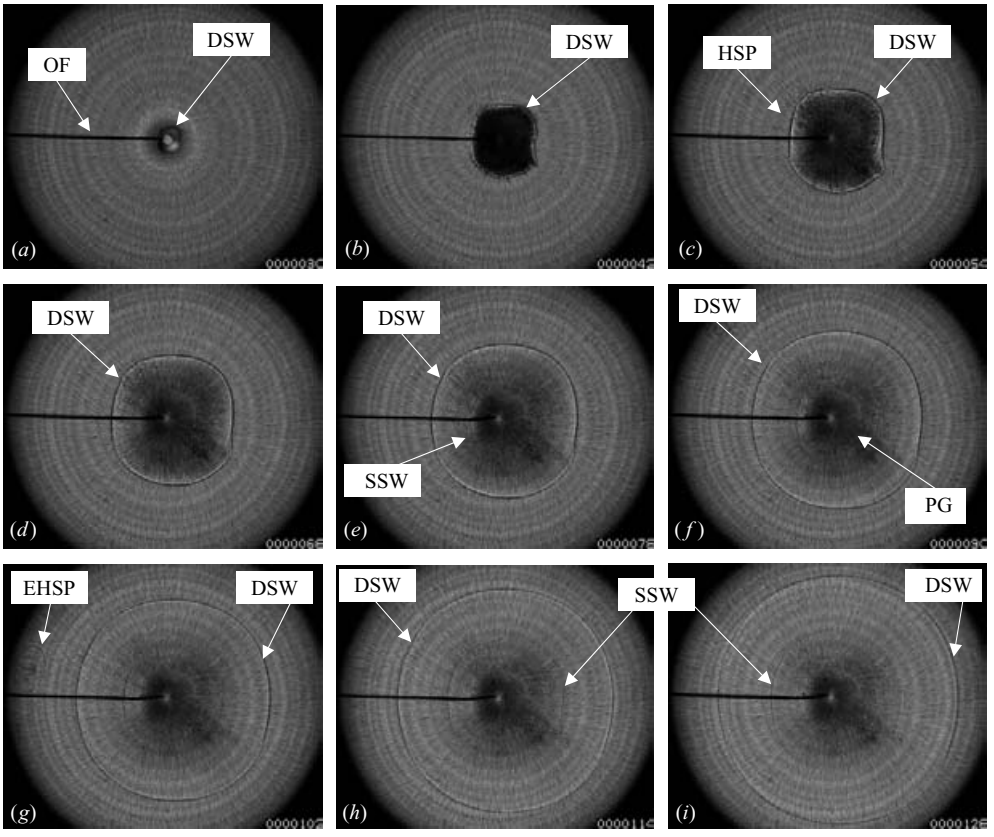

FIGURE 8. Nine frames of time-resolved high-speed shadowgraph visualization of diverging spherical shock wave after base ignition of 5.0 mg conical silver azide pellet in air at ambient pressure 100.35 kPa: (*a*) 3 μs; (*b*) 15 μs; (*c*) 27 μs; (*d*) 39 μs; (*e*) 51 μs; (*f*) 63 μs; (*g*) 75 μs; (*h*) 87 μs; (*i*) 99 μs. DSW, diverging shock wave; EHSP, explosion of high-speed particles; HSP, high-speed particles; OF, optical fibre; PG, product gases; SSW, secondary shock wave.

was produced by a slight asymmetry in reflection of the spherical shock wave from the test section. In figure 11, small deformation of the converging shock increases and $\Delta R/R$ becomes larger with the shock wave propagation, which is due to instability of the converging shock waves. Although interaction with the product gases produced a sudden increase of ΔR for $R/R_0 < 0.15$, deformation of the converging shock front did not remain constant after the interaction, but amplified with the shock propagation, indicating the growing instability. The Kontorovich stability limit may be encountered near the converging centre for shocks strong enough to cause dissociation/ionization (Menikoff & Plohr 1989). In the present case, the maximum converging shock Mach number is less than 2.5 (figure 12), so this kind of instability should not occur.

The average speed of the converging spherical shock wave was derived from the location of the shock front at the given time instant of the time-resolved video recording. Figure 12(*a*) shows the variation of the imploding shock Mach number with normalized radius evaluated from a single high-speed visualization. For the same experiment, the measured wall pressures are shown in figure 3(*b*). The converging spherical shock wave in figure 12(*a*) was considered after interaction with the secondary shock wave (at $t = 185$ μs and radius 61.5 mm or $R/R_0 = 0.82$ shown in figure 10)

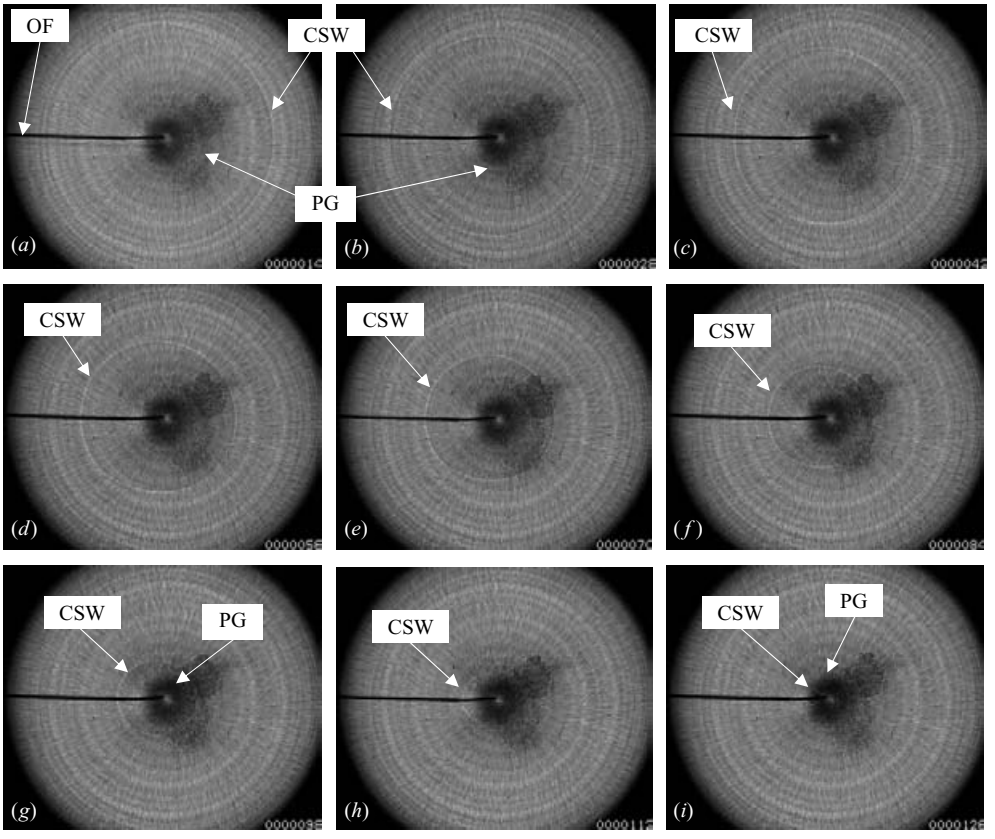

FIGURE 9. Nine frames of time-resolved high-speed shadowgraph visualization of converging spherical shock wave after base ignition of 5.0 mg conical silver azide pellet in air at ambient pressure 100.35 kPa: (*a*) 201 μs; (*b*) 215 μs; (*c*) 229 μs; (*d*) 243 μs; (*e*) 257 μs; (*f*) 271 μs; (*g*) 285 μs; (*h*) 299 μs; (*g*) 313 μs. CSW, converging shock wave; OF, optical fibre; PG, product gases.

and before moving into the gas cloud of detonation products. During the implosion process, the shock speed increases toward the centre. The experimental result in figure 12(*a*) is compared with the ray shock theory based on the Chester–Chisnell–Whitham (CCW) method (Whitham 1974). It is also compared with the prediction of the Guderley theory (1942) in a log–log plot of the normalized converging shock radius against the normalized time measured relative to the arrival time of the shock at the centre in figure 12(*b*). The slope of the plot corresponds to the similarity exponent n of the Guderley theory (1942):

$$\frac{R}{R_0} = \left(1 - \frac{t}{t_c}\right)^n, \tag{3}$$

where t_c is the time when the converging shock arrives at the centre. The experimental best curve fit provides $n = 0.738$ with a correlation coefficient of 0.998, which compares reasonably with Guderley's similarity exponent $n = 0.717$. Although agreements were fair, the theories overestimate the shock speed since, in our experiment, the imploding shock wave propagates in the flow field produced by the diverging blast wave. The CCW method, which agreed very well with Guderley's self-similarity solution (Whitham 1974), assumes a uniform quiescent gas in front of the imploding shock

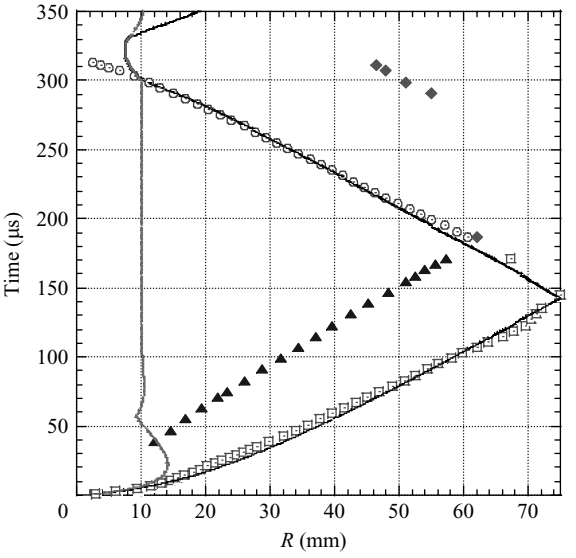

FIGURE 10. Wave diagram of propagation of diverging and converging spherical shock waves in the test section induced by explosion of 5.0 mg conical silver azide pellets. ⊡, Shock front, experiment 1006; ▲, secondary shock wave, experiment 1006; ⊙, shock front, experiment 1007; ◆, secondary shock wave, experiment 1007; —, shock front, numerical; grey line, product gases numerical.

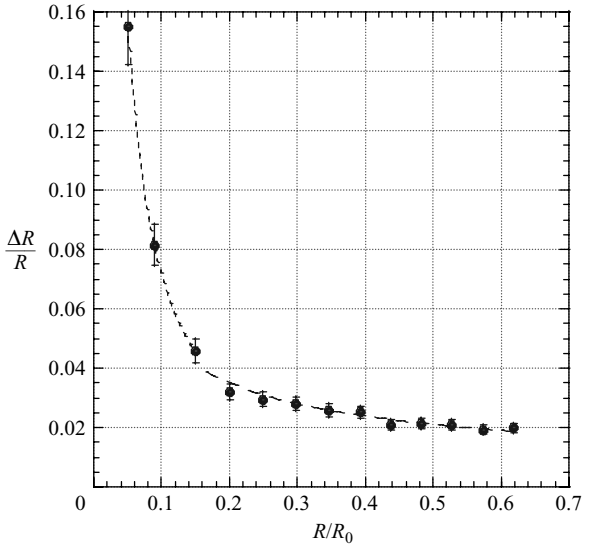

FIGURE 11. Deformation of converging spherical shock front versus radius.

wave, whereas an unsteady flow exists in the experiments with intense real gas and non-uniformity effects. This non-uniform flow into which the imploding shock propagated was clearly observable in interferograms of figure 4 and in pressure measurements of figure 3(*b*). The gradual increase in pressure behind the secondary shock wave in the pressure measurements in figure 3(*b*), between 224 μs and 400 μs, refers to the flow toward the wall. Good agreement was obtained when this flow field ahead of

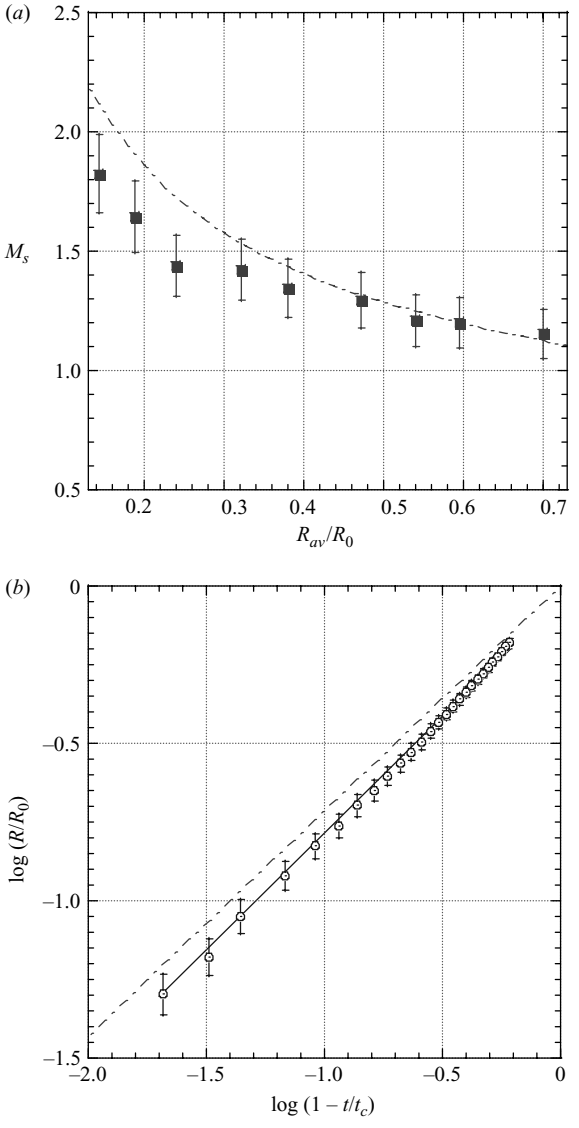

FIGURE 12. (*a*) Variation of converging spherical shock Mach number versus radius, ■, experiment 1007; –·–, ray shock theory. (*b*) Log–log plot of the converging shock radius versus the time measured relative to the arrival time of the shock at the centre, ○, experiment 1007; —, best linear curve fit of experimental results; –·–, Guderley theory.

the converging shock wave was inherently taken into account in numerical simulation, as seen in figure 10.

4. Summary

In order to produce converging spherical shock waves, an aspheric transparent test section with a 150 mm inner diameter spherical cavity was designed and constructed. The importance of quantitative holographic interferometric and time-resolved flow visualization as diagnostic methods, and the essential need for transparency of the

test section were discussed. Pressure measurements at two facing points over the test section's wall confirmed, to a certain degree, that explosions were produced at the centre, nonetheless, the observations revealed non-uniformities in the shock front. To produce uniform spherical shock waves, several alternative modes were tried: a cylindrical silver azide pellet was laser-ignited on both sides; various shapes of pellets were examined. It is concluded that conically shaped pellets ignited at their base produced the minimum deviation in shock front from spherical shape. After reflection of diverging shock waves from the test section spherical wall, converging spherical shock waves were produced, maintaining their symmetry up to the encounter with detonation products gas cloud. The convergence and acceleration of the spherical shock waves in the test section were studied, and effects of the flow field ahead of the converging shock waves and of the product gases on the converging shock waves were discussed. The deformation of the converging spherical shock front increased with the shock wave propagation, which refers to the instability of the converging shock waves.

The authors wish to express their thanks to Mr H. Hayasaka of the Interdisciplinary Shock Wave Research Centre, for the enthusiasm he showed in polishing of the test section. Dr H. Tanaka and Professor T. Saito kindly provided numerical code for silver azide blast wave properties. Professor J. Falcovitz has made valuable comments and editing suggestions. Fruitful discussions with Dr H. Kleine, and Professor P. Voinovich are acknowledged with thanks.

REFERENCES

Apazidis, N. & Lesser, M. B. 1996 On generation and convergence of polygonal-shaped shock waves. *J. Fluid Mech.* **309**, 301–319.

Apazidis, N., Lesser, M. B., Tillmark, N. & Johansson, B. 2002 An experimental and theoretical study of converging polygonal shock waves. *Shock Waves* **12**, 39–58.

Baker, W. E. 1973 *Explosions in Air*. University of Texas Press.

Butler, D. S. 1954 Converging spherical and cylindrical shocks. *Rep. No.* 54/54 Armament Research and Development Establishment, Ministry of Supply, Fort Haltstead, Kent, GB.

Etoh, T. G. 2002 Progress beyond ISIS: combined triple-ISIS camera, video trigger and terraced image sensor. *Proc. SPIE* **4948**, 1–8.

Gardner, J. H., Book, D. L. & Bernstein, I. B. 1982 Stability of imploding shocks in the CCW approximation. *J. Fluid Mech.* **114**, 41–58.

Glass, I. I. 1972 Appraisal of UTIAS implosion-driven hypervelocity launchers and shock tubes. *Prog. Aerospace Sci.* **13**, 223–291.

Glass, I. I. & Sislian, J. P. 1994 *Nonstationary Flows and Shock Waves*. Oxford Science.

Guderley, G. 1942 Starke kugelige und zylindrische Verdichtungsstoesse in der Naehe des Kugelmittepunktes bzw. der Zylinderachse. *Luftfahrtforschung* **19**, 302–312.

Hosseini, S. H. R., Onodera, O. & Takayama, K. 1999 Stability of converging cylindrical shock waves in a vertical annular coaxial diaphragmless shock tube. *Trans. Japan. Soc. Aeronaut. Space Sci.* **42**, 19–26.

Hosseini, S. H. R., Onodera, O. & Takayama, K. 2000 Characteristics of an annular vertical diaphragmless shock tube. *Shock Waves* **10**, 151–158.

Hosseini, S. H. R. & Takayama, K. 2001 Study of shock wave focusing and reflection over symmetrical axis of a compact vertical coaxial diaphragmless shock tube. *Proc. 23rd Intl Symp. Shock Waves, The University of Texas at Arlington, USA*, pp. 1550–1557.

Kleine, H., Dewey, J. M., Ohashi, K., Mizukaki, T. & Takayama, K. 2003 Studies of the TNT equivalence of silver azide charges. *Shock Waves* **13**, 123–138.

Knystautas, R., Lee, B. H. & Lee, J. H. S. 1969 Diagnostic experiments on converging detonations. *Phys. Fluids Suppl.* **1**, 165–168.

Menikoff, R. & Plohr, B. J. 1989 The Riemann problem for fluid flow of real materials. *Rev. Mod. Phys.* **61**, 75–130.

Mizukaki, T. 2001 Quantitative visualization of shock wave phenomena. PhD thesis, Tohoku University, Japan.

Nagayasu, N. 2001 Study of characteristics of micro-explosions. PhD thesis, Tohoku University, Japan.

Payne, R. B. 1957 A numerical method for a converging cylindrical shock. *J. Fluid Mech.* **2**, 185–200.

Perry, R. W. & Kantrowitz, A. 1951 The production and stability of converging shock waves. *J. Appl. Phys.* **22**, 878–886.

Saito, T. & Glass, I. I. 1982 Temperature measurements at an implosion focus. *Proc. R. Soc. Lond.* A **384**, 217–231.

Saito, T. & Glass, I. I. 1984 Applications of random-choice method to problems in gas dynamics. *Prog. Aerospace Sci.* **21**, 201–247.

Schwendeman D. W. 2002 On converging shock waves of spherical and polyhedral form. *J. Fluid Mech.* **454**, 365–386.

Schwendeman D. W. & Whitham G. B. 1987 On converging shock waves. *Proc. R. Soc. Lond.* A **413**, 297–311.

Stanyukovich, K. P. 1960 *Unsteady Motion of Continuous Media*. Pergamon.

Takayama, K. 1983 Application of holographic interferometry to shock wave research. *Proc. SPIE* **398**, 174–181.

Takayama, K., Kleine, H. & Grönig, H. 1987 An experimental investigation of the stability of converging cylindrical shock waves in air. *Exps. Fluids* **5**, 315–322.

Tanaka, K. 1986 Detonation properties of high explosive calculated by revised Kihara–Hikita equation of state. 18*th Intl Symp. Detonation*, *NSWC MP*, pp. 548–557.

Tanaka, K. 2000 Blast wave properties computed by the revised Kihara–Hikita equation of state. *Proc. 14th Intl Mach Reflection Symp. Shock Wave Research Centre, Institute of Fluid Science, Tohoku University*, pp. 258–264.

Terao, K. 1983 Experimental study on cylindrical and spherical implosions. *Japan J. Appl. Phys.* **22**, 446–453.

Van Dyke, M. & Guttmann, A. J. 1982 The converging shock wave from a spherical or cylindrical piston. *J. Fluid Mech.* **120**, 451–462.

Wang, J. C. T. 1982 On the theory of imploding shocks *J. Appl. Math. Phys.* **33**, 53–62.

Watanabe, M., Onodera, O. & Takayama, K. 1995 Shock wave focusing in a vertical annular shock tube. In R. Brun & L. Z. Dumitrescu (ed.), *Shock Waves @ Marseille IV*, pp. 99–104. Springer.

Whitham, G. B. 1974 *Linear and Nonlinear Waves*. John Wiley.

Yamanaka, T. 1972 An investigation of secondary injection thrust vector control. *Tech. Rep. of National Aerospace Laboratory* TR-286T. Chofu, Tokyo, Japan.